6-20-2003

Microstructure evolution of Al–Mg–B thin films by thermal annealing

Y. Tian
Iowa State University

Alan P. Constant
Iowa State University, alcon@iastate.edu

Chester C. H. Lo
Iowa State University

James W. Anderegg
Iowa State University, anderegg@ameslab.gov

Alan M. Russell
Iowa State University, russell@iastate.edu

See next page for additional authors

Microstructure evolution of Al–Mg–B thin films by thermal annealing

Abstract
The growth of Al–Mg–B thin films on SiO2/Si(100) substrates was performed by nanosecond pulsed laser deposition at three different substrate temperatures (300 K, 573 K, and 873 K). The as-deposited films were then annealed at 1173 K or 1273 K for 2 h. X-ray photoelectron spectroscopy,x-ray diffraction(XRD), and atomic force microscope were employed to investigate the effects of processing conditions on the composition, microstructure evolution, and surface morphology of the Al–Mg–B films. The substrate temperatures were found to affect the composition of as-deposited films in that the Mg content decreases and C content increases at higher substrate temperatures, in particular for the 873 K-deposited film.XRD results show that the as-deposited films were amorphous, and this structure may be stable up to 1173 K. Annealing at 1273 K was found to fully crystallize the room temperature and 573 K-deposited Al–Mg–B films with the formation of the polycrystalline orthorhombic AlMgB14 phase, accompanied by the development of a pronounced (011) preferred orientation. Nevertheless, high C incorporation in the 873 K-deposited Al–Mg–B film inhibits the crystallization and the amorphous structure remains stable even during 1273 K annealing. The presence of Si in the room-temperature-deposited 1273 K-annealed film due to the interdiffusion between the substrate and film leads to the formation of an additional tetragonal α-FeSi2 phase, which is thought to cause the surface cracking and microstructural instability observed in this film.

Keywords
Ames Laboratory, Thin film structure, Annealing, Thin film growth, X-ray diffraction, Crystal structure

Disciplines
Metallurgy

Comments
The following article appeared in Journal of Vacuum Science and Technology A 21, 1055 (2003); and may be found at doi:10.1116/1.1586274.

Authors
Y. Tian, Alan P. Constant, Chester C. H. Lo, James W. Anderegg, Alan M. Russell, J. E. Snyder, and P. Molian

JVSTA Journal of Vacuum Science & Technology A

Microstructure evolution of Al–Mg–B thin films by thermal annealing

Y. Tian, A. Constant, C. C. H. Lo, J. W. Anderegg, A. M. Russell, J. E. Snyder, and P. Molian

Citation: Journal of Vacuum Science & Technology A **21**, 1055 (2003); doi: 10.1116/1.1586274
View online: http://dx.doi.org/10.1116/1.1586274
View Table of Contents: http://scitation.aip.org/content/avs/journal/jvsta/21/4?ver=pdfcov
Published by the AVS: Science & Technology of Materials, Interfaces, and Processing

Microstructure evolution of Al–Mg–B thin films by thermal annealing

Y. Tian[a)]
Department of Materials Science and Engineering, Iowa State University, Ames, Iowa 50011

A. Constant
Microelectronics Research Center and Department of Materials Science and Engineering, Iowa State University, Ames, Iowa 50011

C. C. H. Lo and J. W. Anderegg
Ames Laboratory, United States Department of Energy, Ames, Iowa 50011

A. M. Russell and J. E. Snyder
Department of Materials Science and Engineering and Ames Laboratory, United States Department of Energy, Iowa State University, Ames, Iowa 50011

P. Molian
Department of Mechanical Engineering, Iowa State University, Ames, Iowa 50011

(Received 9 January 2003; accepted 5 May 2003; published 20 June 2003)

The growth of Al–Mg–B thin films on SiO_2/Si(100) substrates was performed by nanosecond pulsed laser deposition at three different substrate temperatures (300 K, 573 K, and 873 K). The as-deposited films were then annealed at 1173 K or 1273 K for 2 h. X-ray photoelectron spectroscopy, x-ray diffraction (XRD), and atomic force microscope were employed to investigate the effects of processing conditions on the composition, microstructure evolution, and surface morphology of the Al–Mg–B films. The substrate temperatures were found to affect the composition of as-deposited films in that the Mg content decreases and C content increases at higher substrate temperatures, in particular for the 873 K-deposited film. XRD results show that the as-deposited films were amorphous, and this structure may be stable up to 1173 K. Annealing at 1273 K was found to fully crystallize the room temperature and 573 K-deposited Al–Mg–B films with the formation of the polycrystalline orthorhombic $AlMgB_{14}$ phase, accompanied by the development of a pronounced (011) preferred orientation. Nevertheless, high C incorporation in the 873 K-deposited Al–Mg–B film inhibits the crystallization and the amorphous structure remains stable even during 1273 K annealing. The presence of Si in the room-temperature-deposited 1273 K-annealed film due to the interdiffusion between the substrate and film leads to the formation of an additional tetragonal α-$FeSi_2$ phase, which is thought to cause the surface cracking and microstructural instability observed in this film.
[DOI: 10.1116/1.1586274]

I. INTRODUCTION

The mechanical, electrical, and thermal properties of boron-rich borides make them a productive object of study from both scientific and engineering perspectives. They are stable refractory semiconductors, and the fabrication of boron-rich boride-based electronic devices was recently reported.[1,2] They possess large Seebeck coefficients and low thermal conductivity, which suggests their possible use in thermoelectric energy conversion.[3,4] Due to the large neutron capture cross section of ^{10}B, boron-rich borides have found application in fission reactors for the absorption of thermal neutrons and as solid-state neutron detectors.[5,6] Boron-rich borides have also been recognized for their high hardness, low density, and chemical inertness, make attractive materials for cutting tools and wear-resistant coatings.[7,8]

The basic structural feature of boron-rich borides is the B_{12} boron icosahedral cluster, in which each boron atom shares three valence electrons with five neighboring boron atoms, leading to electron-deficient, three-center intraicosahedral bonding.[3] These B_{12} icosahedra are either linked directly to one another or are connected via a single B or non-B atoms, forming a large variety of open frameworks, which distinguishes the boron-rich borides from conventional semiconductors with simple translational symmetry and from amorphous semiconductors with short-range order.

There has been considerable interest in studying boron-rich borides in thin-film form, especially B_4C, B_4N, and boron suboxide ($B_xO, x>1$) for potential application as hard coatings, due to their extraordinary mechanical properties. Boride films have been prepared by various deposition methods: electron cyclotron resonance microwave plasma assisted thermal evaporation,[9] hot filament chemical vapor deposition,[10] reactive rf magnetron sputtering,[11,12] pulsed dc magnetron sputtering,[13] dual ion beam deposition,[14] vacuum (cathodic) arc deposition,[15] and pulsed laser deposition.[16] Boride films obtained in prior work were usually amorphous,

[a)]Author to whom correspondence should be addressed at: Department of Materials Science and Engineering, Iowa State University, 3053, Gilman Hall, Ames, IA 50011; electronic mail: ytian@iastate.edu

TABLE I. Density and hardness of selected hard materials.

	Density (g/cm^3)	Hardness (GPa)
C (diamond)	3.52	70
BN (cubic)	3.48	45–50
SiC	3.22	24–28
TiB_2	4.50	30–33
WC	15.72	23–30
TiC	4.93	28–29
Si_3N_4	3.19	17–21
$AlMgB_{14}$	2.66	32–35
$AlMgB_{14}$+Si	2.67	35–40
$AlMgB_{14}$+TiB_2	2.70	40–46

and the mechanical properties vary with different deposition techniques. Hardnesses of 25–30 GPa and elastic moduli of 180–300 GPa have been observed. Furthermore, oxidation at the free surfaces of these boride films tends to grow a glassy B_2O_3 layer, which reacts spontaneously with ambient water vapor to form a thin boric acid (H_3BO_3) boundary film. This boundary film can have a friction coefficient as low as 0.05, thus providing an excellent self-lubricant.[17] For these reasons, boron-rich boride films are emerging as an intriguing class of superhard materials with a wide range of applications.

Recently, a ternary boride $AlMgB_{14}$ with extreme hardness and high thermal stability was developed by Ames Laboratory scientists.[8] The hardness of $AlMgB_{14}$ with submicron-scale grain size ranges between 32 and 35 GPa, and the hardness of $AlMgB_{14}$ containing 5 to 30 mol % additives lies in the range 35–46 GPa, with the highest hardness observed in material containing 30% TiB_2 of a mean phase size of $\sim$200 nm. A hardness of 45 GPa is comparable to the hardness of cubic-BN (Table I), placing this material in the superhard category. Moreover, the cost of $AlMgB_{14}$ is projected to be about five to ten times lower than the costs of cubic-BN and diamond. As shown in Fig. 1, the crystal structure of $AlMgB_{14}$ is a body-centered orthorhombic arrangement, space group Imam, with lattice constants $a=0.5848$ nm, $b=0.8112$ nm, and $c=1.0312$ nm. The unit cell contains 64 atoms and is based on four B_{12} icosahedral units centered at (0, 0, 0), (0, 0.5, 0.5), (0.5, 0, 0), and (0.5, 0.5, 0.5) within the unit cell, while the remaining eight B atoms lie outside the icosahedra, bonding to the icosahedral B atoms and to the intericosahedral Al atoms occupying a four-fold position at (0.250, 0.750, and 0.250) and the intericosahedral Mg atoms occupying a four-fold position at (0.250, 0.359, and 0).[18,19] Crystallographic studies indicate that the metal sites are not fully occupied in the $AlMgB_{14}$ lattice, so that the true stoichiometry may be $Al_{0.75}Mg_{0.78}B_{14,}$ which is the necessary consequence of the electron deficiency in the valence band.[20] In addition, single crystal $AlMgB_{14}$ exhibits intrinsic *n*-type transport behavior,[21] and hot-pressed $AlMgB_{14}$ has a higher electrical conductivity ($\sim$80 to 1500 $\Omega^{-1}\,m^{-1}$) than most traditional hard materials.[22] Recent band structure calculations[23] performed on these borides suggest that the hardness may change as the nature of the electronic states at the Fermi level changes, hence, it appears that doping may play a vital role in determining the physical properties. More recently, dry machining tests in which bulk $AlMgB_{14}$ was used as the cutting tool, showed an unusual absence of tool heating, suggesting that this orthorhombic boride might possess very low thermal conductivity.[24]

Its high hardness, high thermal stability, and desirable electrical and thermal properties suggest the potential utilization of $AlMgB_{14}$ as self-lubricating, wear-resistant, and protective coatings for cutting tools[25] and mechanical components ranging in size from massive mining and materials handling applications to microelectromechanical systems.[26] It was believed that the superhardness of bulk $AlMgB_{14}$ is determined by its nanocrystalline multiphase structure since single crystal $AlMgB_{14}$ has hardness of only 28 GPa.[8] Veprek refers to this microstructural contribution to hardness in the nanocomposite as ''extrinsic hardness.'' [27] Thus, the appropriate crystalline microstructure is thought to be crucial for achieving extreme hardness in thin-film form. The primary focus of this research was devoted to preparing crystalline $AlMgB_{14}$ thin films and examining the influence of processing routes on the composition, microstructure evolution, and surface morphology of polycrystalline boride films.

II. EXPERIMENTAL PROCEDURE

$AlMgB_{14}$ films were deposited on thermally oxidized Si (100) substrates by a turbopumped Neocera pulsed laser deposition (PLD) system. In this PLD system, a KrF excimer laser beam ($\lambda=248$ nm, pulse energy 70 mJ, pulse duration <50 ns, and repetition rate 10 Hz) was delivered to the hot-pressed baseline $AlMgB_{14}$ target with an energy density of $\sim$1.2 J/cm^2 through a focusing lens to generate a plasma plume in a high-vacuum chamber (typical base pressure $<3\times10^{-6}$ Torr). The target contained some oxygen impurity in the form of $MgAl_2O_4$ spinel phase. The substrate was placed parallel to the target, and the distance between the substrate and target was 7 cm. Depositions were carried out at three different substrate temperatures (room temperature, 573 K, and 873 K), and the film thickness was controlled by the deposition rate of 0.014 Å/pulse and the total deposition time was 3 h. After deposition, all as-deposited films were isothermally annealed at 1173 K or 1273 K for 2 h, the annealing process was conducted in a NRC 2940 high-temperature vacuum furnace, which was evacuated below a base pressure of 2×10^{-6} Torr and then backfilled with yttrium-gettered Ar to ambient pressure prior to annealing. The temperature ramp rate was set at 17 °C/min.

X-ray diffraction (XRD) patterns of the films were collected using a Scintag θ–2θ x-ray diffractometer with Cu $K\alpha$ radiation. Surface topography and roughness of the films were studied using a Digital Instruments Dimension 3100 atomic force microscope (AFM) operated in tapping mode with a silicon pyramidal probe. The residual stresses of as-deposited films were determined by measuring the curvature of the film–substrate combination with an AFM and by using the Stoney formula:[28]

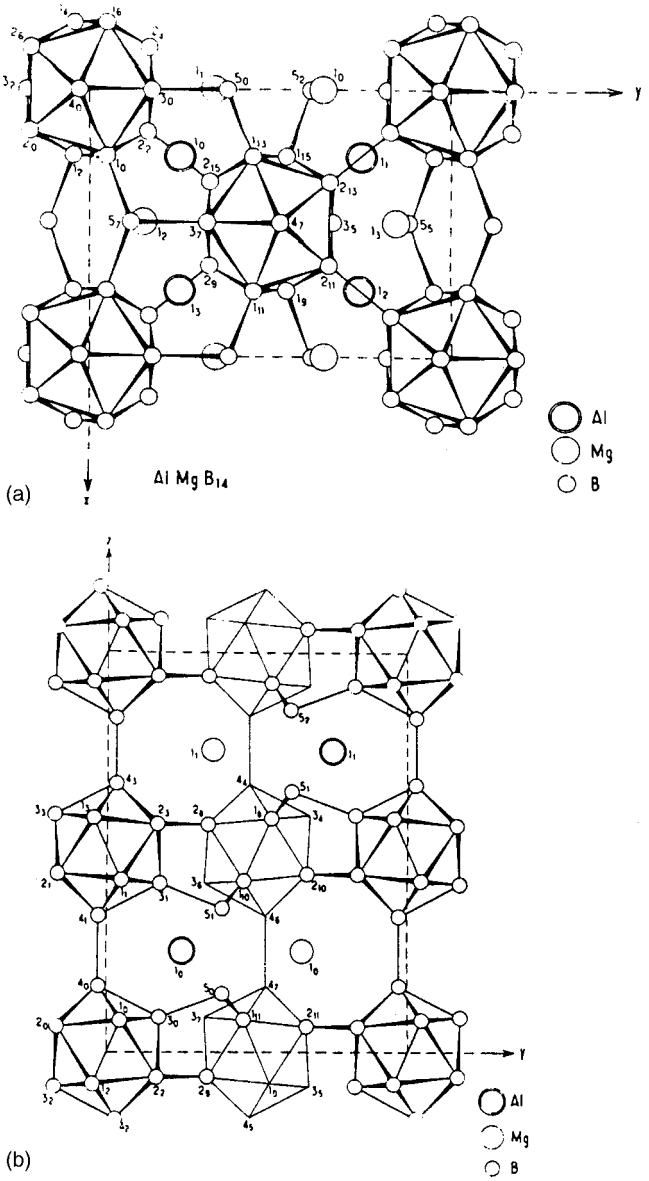

FIG. 1. Crystal structure of orthorhombic $AlMgB_{14}$. (a) Projection on the ab plane. (b) Projection on the bc plane.

$$\sigma_f = \frac{E_s d_s^2}{6R(1-\nu_s)d_f}, \tag{1}$$

where σ_f refers to the biaxial stress of the film, E_s, ν_s, and d_s are Young's modulus, Poisson's ratio, and the thickness of the substrate, respectively, d_f and R are the thickness of the film and radius of curvature of the film–substrate composite. The film thickness was measured by an AFM.

X-ray photoelectron spectroscopy (XPS) (PHI™ Physical Electronics 5500 Multitechnique ESCA system) with monochromatic Al $K\alpha$ radiation (1486.6 eV) and standard Mg/Al sources was used to determine the compositional information of the films. The Au $4f_{7/2}$ and Cu $2p_{3/2}$ excitations at 84.0 eV and 932.6 eV were used for energy calibration, and the atomic concentration was calculated by using the sensitivity factors provided with the PHI™ acquisition software. Analysis spot size can be varied from $1\times0.8\ \text{mm}^2$ to $0.4\times0.4\ \text{mm}^2$ with energy resolution of better than 0.5 eV. The base pressure for the analyzer system was less than 3×10^{-10} Torr. The films were subjected to an Ar^+ ion bombardment using 4 kV Ar^+ ions at 3 μA total target current to remove the surface oxide layer before the XPS analysis.

III. RESULTS AND DISCUSSION

PLD was chosen to fabricate $AlMgB_{14}$ films in this work because it is one of the most widely used physical vapor deposition (PVD) methods for depositing multicomponent thin films, with good capability of accurately preserving the target stoichiometry in the film due to congruent ablation induced by high-intensity laser irradiation of the target.[29] The atomic concentrations of the constituents of as-deposited films are shown as a function of substrate temperatures in Table II. It can be seen that the atomic ratio of Al, Mg, and B for the film deposited at room temperature is very close to 1:1:14 stoichiometry with ~2.3 at. % Al in excess. The oxygen content (9.53 at. %) is higher than expected in view of the vacuum level achieved (base pressure $\sim8\times10^{-7}$ Torr), which may be due to the high affinity of Al and Mg for oxygen and low deposition rate caused by low laser energy (70 mJ). Low laser power was used to prevent particulate incorporation into the growing films. The oxygen partial pressure was measured using a residual gas analyzer at a base pressure of 6×10^{-7} Torr, and oxygen partial pressure was close to 1×10^{-7} Torr. At 10^{-6} Torr partial pressure, the atomic flux of any gaseous species is about a monolayer per second, hence, oxygen incorporation levels can be quite high in the films if the sticking coefficient of oxygen is relatively high. Baking out the chamber could reduce the oxygen content, but some degree of contamination in the films is unavoidable in light of the $MgAl_2O_4$ content of the $AlMgB_{14}$ target. The Fe in the films arises from a steel mill vial and media wear debris introduced into the target material during the high-energy ball mill process used to produce the target.[8] For the film deposited at 573 K, the Al, Mg, and B contents were found to deviate slightly from 1:1:14 stoichiometry with ~2.3 at. % excess Al, and ~1.1 at. % Mg deficiency. However, in contrast to the room-temperature and 573 K-deposited films, the 873 K-deposited film showed a marked increase of C content, jumping from ~2 at. % (the practical noise level for C in the XPS measurement) to 13 at. %. Meanwhile, the amount of Mg incorporation drops to only 2.08 at. %, a sharp decrease from the 4.98 at. % Mg of fully stoichiometric film deposited at room temperature. Since Mg has a high vapor pressure over a broad temperature range, one might expect the Mg content to decrease with rising substrate temperature.

The six-fold increase in C content in the 873 K-deposited film is attributed to significant outgassing and decomposition at 873 K of some C-containing molecules or volatile organic compounds adsorbed on the chamber wall and O rings. Furthermore, a resputtering effect is believed to be another contributing factor, i.e., the growing film was sputtered somewhat by the highly energetic (~200–1000 kT) impinging species (mixed ions, atoms, and molecules), leading to a dy-

TABLE II. Composition of as-deposited Al–Mg–B films.

Substrate temperature (K)	B (at. %)	Al (at. %)	Mg (at. %)	O (at. %)	Fe (at. %)	C (at. %)
300	71.46	7.41	4.98	9.53	4.67	1.95
573	69.13	7.24	3.82	12.56	4.71	2.55
873	55.16	9.68	2.08	14.36	5.30	13.42

namic balance between the deposition and sputtering processes. At the elevated substrate temperatures, the enhanced surface mobility of the C atoms promotes their reaction with Fe atoms to form carbide; thus, during deposition, the resputtering effect on C atoms in the 873 K-deposited film is weaker than that in the room-temperature and 573 K-deposited films, presumably because breaking the strong Fe—C bond in carbide formed in the film requires much higher energy than noncarbide forming films in which C atoms are loosely linked to the amorphous matrix. As a result, the 873 K-deposited film has much greater C content.

XPS compositional analysis was also performed on the films annealed at 1273 K. Although there is a negligibly small amount of Si present in the as-deposited films, the 1273 K-annealed films showed the presence of Si irrespective of substrate temperatures, and the Si concentration was found to decrease monotonically from about 9 at. % to 4.3 at. % as substrate temperatures increased (Fig. 2). The presence of Si in the 1273 K-annealed films is not particularly surprising in a thin film with a SiO_2/Si substrate. The thermally activated migration of Si from the substrate and/or its oxide layer into the films during annealing at 1273 K indicates the failure of the amorphous SiO_2 layer as a diffusion barrier at this temperature. It is well known that substrate temperature plays an important role in determining thin-film microstructure, therefore, the effect of substrate temperatures on the Si concentration shown in Fig. 2 can be attributed to different microstructures associated with different substrate temperatures. At low substrate temperatures, owing to limited surface mobility, there is not enough time for adatoms to find positions of energy minima before being constrained by subsequently deposited atoms, thus these atoms are ''quenched'' onto the substrate surface, facilitating the formation of nonequilibrium film structure with a high defect density. The various defects, such as vacancies, pinholes, and microporosity, etc., are believed to provide an effective pathway for faster Si outdiffusion. For the same deposition rate but higher substrate temperatures, reduced defect concentrations and denser structures can be expected, hence, effectively retarding Si migration into the films. Consequently, film deposited at a higher substrate temperature would be expected to contain less Si after annealing, as shown in Fig. 2.

Figure 3(a) shows the XRD patterns for the room-temperature as-deposited film, the room-temperature-deposited 1173 K-annealed film and the room-temperature-deposited 1273 K-annealed film. Aside from the Si (200) reflection centered at $2\theta \sim 33°$, the XRD pattern for as-deposited film exhibits no diffraction features; this is indicative of an amorphous or nearly amorphous film structure. Although the Si (200) is a ''forbidden'' peak, it can appear because of growth-induced compressive stress leading to a slight distortion of the Si unit cell from cubic to tetragonal. The XRD pattern for the film annealed at 1173 K remains unchanged compared with the as-deposited film, suggesting that the amorphous structure persists up to 1173 K. Another possibility is that the film has a nanocrystalline structure with extremely fine grain size which cannot be detected by XRD $\theta-2\theta$ scans. Transmission electron microscopy (TEM)-based structural investigations would be needed to further explore this issue. The XRD pattern for the 1273 K-annealed film shows four sharp diffraction peaks originating from the film, indicating that the film has been rendered fully crystalline at this annealing temperature. The peak centered at $2\theta = 17.27°$ can be ascribed to *c*-axis oriented tetragonal α-$FeSi_2$ phase. Three additional peaks centered at 2θ positions of 13.85°, 27.89°, and 42.37° were identified to correspond to (011), (022), and (033) planes of the $AlMgB_{14}$ orthorhombic structure respectively; obviously, a strong (011) crystallographic texture has developed. It should be noted that the intensity ratio of the (022) peak to the (033) peak, $I_{(022)}/I_{(033)}$, is approximately 1:3 and agrees well with the standard $AlMgB_{14}$ powder diffraction pattern, whereas the intensity of the (011) peak relative to that of the (022) and (033) peaks appears to be abnormally faint, which is thought to be a consequence of the special low-angle diffraction geometry for a small thin-film sample.

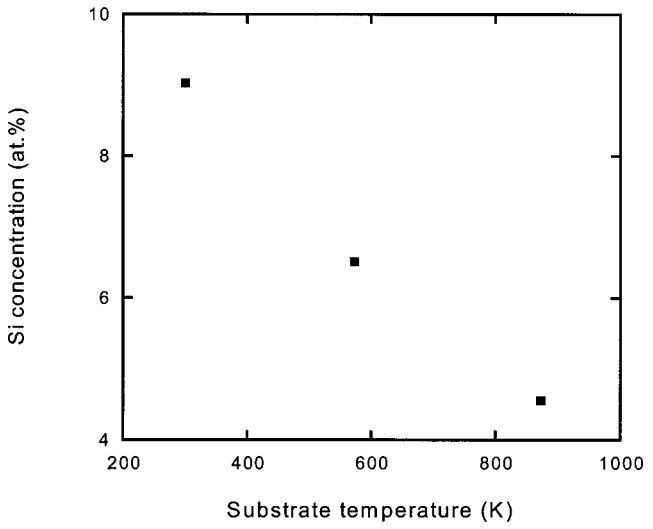

FIG. 2. Relation between Si concentration (at. %) in the 1273 K-annealed films and substrate temperatures during film deposition.

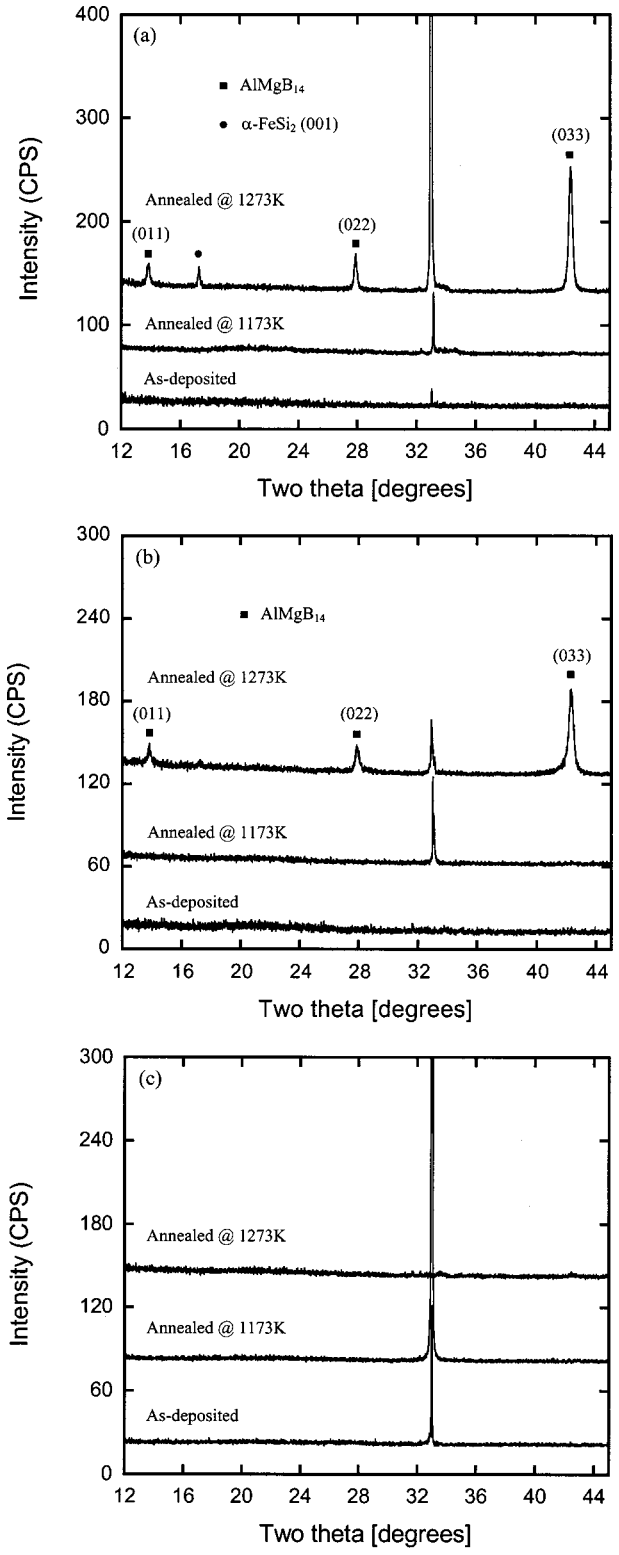

FIG. 3. (a) XRD patterns for the room-temperature as-deposited film, the room-temperature-deposited 1173 K-annealed film and the room-temperature-deposited 1273 K-annealed film. (b) XRD patterns for the 573 K as-deposited film, the 573 K-deposited 1173 K-annealed film, and the 573 K-deposited 1273 K-annealed film. (c) XRD patterns for the 873 K as-deposited film, the 873 K-deposited 1173 K-annealed film, and the 873 K-deposited 1273 K-annealed film.

The XRD patterns for the 573 K as-deposited film, the 573 K-deposited 1173 K-annealed film, and the 573 K-deposited 1273 K-annealed film are presented in Fig. 3(b). The as-deposited film is apparently amorphous, and the film annealed at 1173 K is either amorphous or nanocrystalline. The XRD pattern for the 1273 K-annealed film explicitly shows the $AlMgB_{14}$ orthorhombic structure with the (011) preferred orientation. The peak corresponding to α-$FeSi_2$ phase is barely discernible, probably due to the fact that there is insufficient Si in the 573 K-deposited 1273 K-annealed film (Fig. 2) to allow for formation of substantial amounts of α-$FeSi_2$ phase. Therefore annealing the 573 K-deposited film at 1273 K yields predominantly single-phase $AlMgB_{14}$.

As Table II shows, the room-temperature and 573 K as-deposited films contained 9.53 at.% and 12.56 at.% O respectively, which has the potential to substantially alter the specimen composition and microstructure. The effect of O impurity has been studied in bulk $AlMgB_{14}$.[30] That study demonstrated that O prevents formation of single-phase $AlMgB_{14}$. The O reacts with Al and Mg to form a spinel $MgAl_2O_4$ phase, and if Fe impurity is present from milling wear debris, the O also reacts with Fe to form spinel Fe_3O_4 phase. Hence, a three-phase structure of $AlMgB_{14}$, Fe_3O_4, and $MgAl_2O_4$ typically forms in bulk material with O impurities. TEM analysis of such bulk material shows distinct spinel phases juxtaposed with pure $AlMgB_{14}$ phases; no evidence of quaternary or higher-order compounds was reported. Thus, it is a strong possibility that appreciable amounts of spinel phases also formed in the room-temperature-deposited 1273 K-annealed film and the 573 K-deposited 1273 K-annealed film, although their volume percentages were apparently too low to produce discernible peaks in the XRD patterns.

The XRD patterns for the 873 K as-deposited film, the 873 K-deposited 1173 K-annealed film, and the 873 K-deposited 1273 K-annealed film are shown in Fig. 3(c). Aside from the Si (200) reflection, no diffraction peaks can be observed in any of the three cases, demonstrating that the amorphous structure remains stable even by annealing at 1273 K. Because a significant amount of C impurity gets incorporated into the 873 K-deposited film, it seems likely that C plays a critical role in stabilizing the amorphous structure. In other studies, the presence of C impurity was reported to promote the formation of β-AlB_{12} phase in preference to $AlMgB_{14}$,[21] thus, it appears that the C content in films needs to be as low as possible in order to obtain the orthorhombic $AlMgB_{14}$ structure. It should be pointed out that the presence of a large amount of oxygen (14.36 at.%) in the 873 K-deposited film might be able to further inhibit the formation of crystalline $AlMgB_{14}$ phase because the oxidation of Al, Mg, and B was more energetically favorable, yielding a complex oxide glass structure with B playing the role of network former.[31]

Strong crystallographic textures are commonly observed in polycrystalline thin films grown by PVD techniques. A variety of physical properties are influenced substantially by the film texture.[32–34] Understanding how the texture devel-

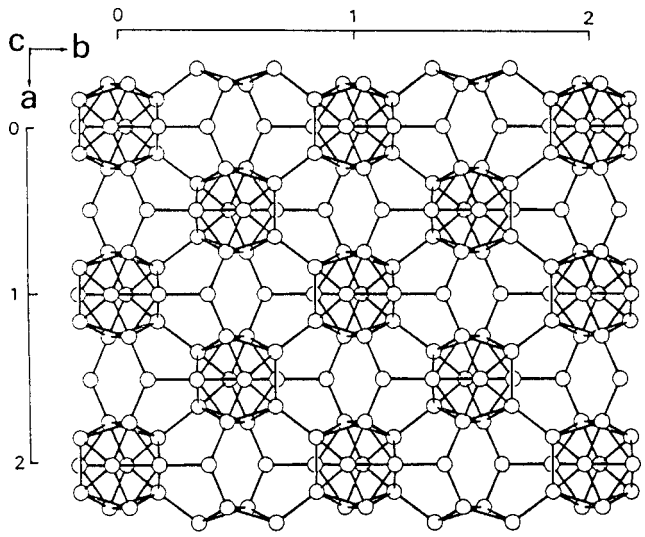

FIG. 4. Icosahedral B_{12} network parallel to the (001) plane of orthorhombic $AlMgB_{14}$ (see Ref. 35).

ops in $AlMgB_{14}$ film, therefore, is necessary for achieving control of its microstructure and properties. The previous study by Higashi *et al.*[35] showed that typical platelike $AlMgB_{14}$ single crystals were bounded by the well-developed (001) plane, indicating that the (001) plane may have the minimum surface energy. In principle, closest-packed planes with the minimum surface energy tend to be aligned parallel to the film surface (fiber texture), however, the XRD results in the present study clearly show the development of the strong (011) texture rather than the (001) texture in the 1273 K-annealed $AlMgB_{14}$ films. This phenomenon can be explained in terms of the following mechanism: Based on the observation of a columnar grain structure by AFM (discussed later), the nucleation of a crystalline $AlMgB_{14}$ phase in an amorphous $AlMgB_{14}$ matrix is presumed to initiate at the substrate surface, the situation is quite similar to heterogeneous nucleation and growth of thin films from a vapor or liquid phase. It is common for vapor-deposited thin films to adopt an orientation that does not correspond with the lowest-energy surface. For example, the {110} planes of body-centered-cubic (bcc) Cr have the lowest surface energy; however, Cr films grown on a substrate which favors three-dimensional (3D) nucleation (poor wetting), adopt a (002) texture so as to expose the {110} lowest-energy facets, while Cr films that completely wet a substrate [two-dimensional (2D) nucleation] grow with {110} texture.[36] In analogy with Cr films, the incoherent interface between a crystalline $AlMgB_{14}$ nucleus and the underlying amorphous SiO_2 layer promotes 3D nucleation and growth due to poor wetting, hence, the (011) texture is preferred since this configuration exposes the lowest-energy (001) facets, thereby minimizing the total interfacial energy in the film.

The (001) texture is beneficial to mechanical properties of $AlMgB_{14}$ film because there are greater numbers of B_{12} icosahedra, and thus a greater number of B—B bonds in the B_{12} network parallel to the (001) plane (Fig. 4), leading to a significantly enhanced hardness on that plane.[35] Consequently, the prevalence of (001) texture in $AlMgB_{14}$ films is thought to be highly desirable for application as hard coatings. According to the aforementioned mechanism for texture evolution, to form the (001) texture depends on the selection of the appropriate substrate material (good substrate wettability). It is essential for the substrate to have the crystal structure and lattice parameters similar to $AlMgB_{14}$ so that the (001) texture may develop as a result of 2D nucleation and growth. This texturing mechanism for $AlMgB_{14}$ film suggests possible benefits from a double deposition: First deposit an ''underlayer'' of $AlMgB_{14}$, which can then be crystallized by annealing to serve as a structural template, followed by a subsequent deposition and annealing of $AlMgB_{14}$ film to establish a (001) texture in the exposed surface.

Figure 5 shows the AFM images of the surface morphologies of $AlMgB_{14}$ films deposited at room temperature before and after 1273 K-annealing. The room-temperature-as deposited film [Fig. 5(a)] displays a smooth surface profile dominated by domed features, the root-mean-square (rms) roughness over a scan area of $2\times2\ \mu m^2$ is about 1.91 nm. For the 1273 K-annealed film [Fig. 5(b)], surface cracks were observed, particularly along the edges of the film, appearing as a mosaic pattern. The film shows a few particles on its surface, which is a typical characteristic of the PLD method. Additionally, the film has become discontinuous by breaking up into islands of irregular shape with lateral size ranging from $\sim$200 nm to 800 nm, it appears that these islands may correspond to a crystalline columnar structure. Such an interpretation is supported by the fact that strong texture has developed in the 1273 K-annealed $AlMgB_{14}$ films. The rms roughness of the 1273 K-annealed film is 15.58 nm over a scan area of $2\times2\ \mu m^2$.

The AFM images of $AlMgB_{14}$ films deposited at 573 K before and after 1273 K-annealing are presented in Fig. 6. The surface of the 573 K-as-deposited film [Fig. 6(a)] shows typical amorphous features with rms roughness as low as 0.92 nm over a scan area of $2\times2\ \mu m^2$, this atomically flat surface is intimately related to the highly energetic incident species produced by laser ablation.[37] The surface of the 1273 K-annealed film [Fig. 6(b)] exhibits sharp spikes, which are thought to be the result of oriented grains ''pushing'' out of the film during crystallization, the rms roughness is 2.05 nm over a scan area of $2\times2\ \mu m^2$; the whole film is continuous and free of cracks.

Surface cracking was found on the room-temperature-deposited 1273 K-annealed $AlMgB_{14}$ film. Because the thermal expansion coefficient of the Si substrate ($\sim4\times10^{-6}$/K) is much less than that of crystalline $AlMgB_{14}$ film ($\sim9\times10^{-6}$/K),[38] a significant tensile stress built up as the film was cooled from the annealing at 1273 K, which is believed to be responsible for the crack formation. This tensile stress can be estimated from the following formula for thermal stress calculation:[28]

$$\sigma_t=\frac{E_f(\alpha_s-\alpha_f)\Delta T}{1-\nu_f}, \tag{2}$$

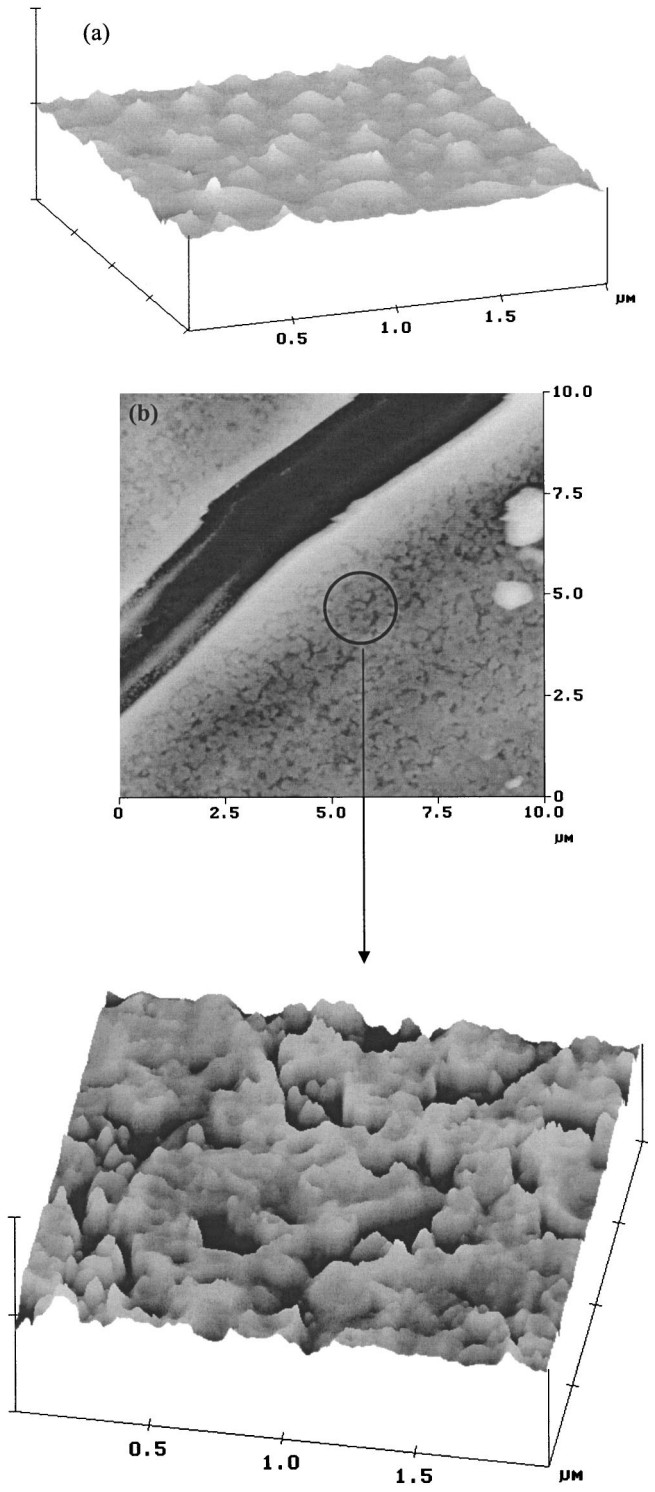

FIG. 5. (a) AFM images of the room-temperature-as deposited $AlMgB_{14}$ film. (b) AFM images of the room-temperature-deposited, 1273 K-annealed $AlMgB_{14}$ film.

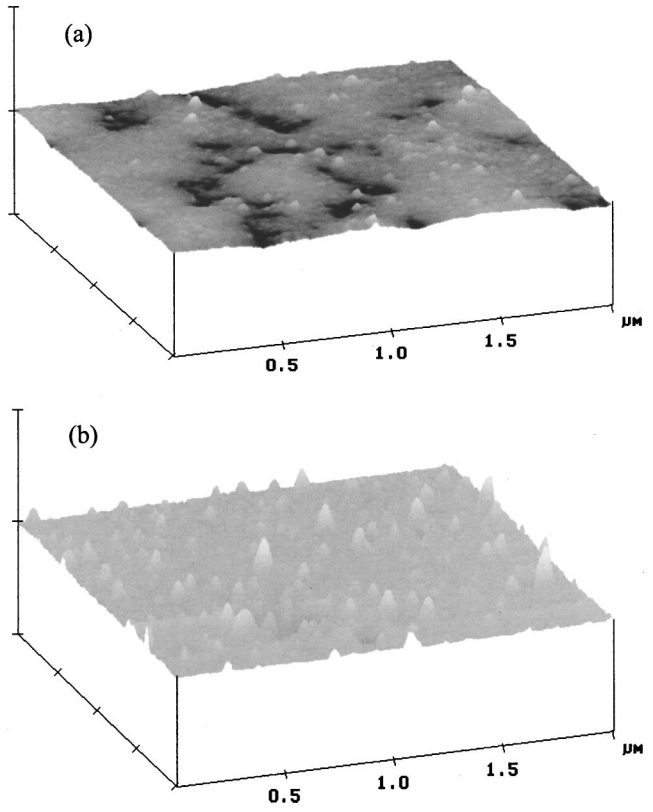

FIG. 6. (a) AFM images of the 573 K-as deposited $AlMgB_{14}$ film. (b) AFM images of the 573 K-deposited, 1273 K-annealed $AlMgB_{14}$ film.

where σ_t is thermal stress of the film, E_f, ν_f, and α_f are Young's modulus, Poisson's ratio, and thermal expansion coefficient of the film, respectively, α_s is thermal expansion coefficient of the substrate; for crystalline $AlMgB_{14}$ film, E_f is about 509 GPa, and ν_f is 0.1,[23] on cooling from 1273 K annealing temperature, the thermal stress would be 2.75 GPa. The compressive intrinsic stresses for the room-temperature and 573 K as-deposited $AlMgB_{14}$ films were about 637 MPa and 278 MPa, respectively, they were relaxed by annealing at 1273 K through thermally activated defects annihilation, therefore, their contribution to the crack formation is negligible.

The 573 K-deposited 1273 K-annealed $AlMgB_{14}$ film, nevertheless, does not show any evidence of surface cracking, even though subjected to a large tensile stress. This phenomenon may be attributable to the different microstructures for the 1273 K-annealed films. The room-temperature-deposited 1273 K-annealed $AlMgB_{14}$ film consists of two phases: orthorhombic $AlMgB_{14}$ phase and tetragonal α-$FeSi_2$ phase, which differ in their thermal expansion coefficients ($\sim 6.7\times 10^{-6}$/K for α-$FeSi_2$).[39] During the cooling period of an annealing cycle, a high strain incompatibility arising from thermal expansion mismatch may develop at the phase boundaries in the presence of tensile stress, therefore, the phase boundary becomes the site for crack initiation and provides an easy path for subsequent crack propagation, resulting in premature intergranular fracture of the film. By contrast, the 573 K-deposited 1273 K-annealed film is comprised of single-phase $AlMgB_{14}$, hence it can withstand much greater tensile stress due to the absence of incompatible strain.

It is interesting to note that surface cracking was also found on the room-temperature-deposited 1173 K-annealed

$AlMgB_{14}$ film, which probably still retains amorphous structure according to the XRD pattern. However, if this is the case, it would be difficult to explain the origin of the high tensile stress responsible for the crack occurrence. Indeed, it seems plausible to assume that a nanocrystalline structure with extremely fine grain size might have formed, even though there is no direct experimental evidence.

Islands with holes in between exposing the substrate were developed in the room-temperature-deposited 1273 K-annealed $AlMgB_{14}$ film, indicating that a microstructural instability has occurred. It is generally assumed that thin films will remain stable during processing and service; however, initially continuous films are not always thermodynamically stable and they can ''dewet'' or uncover the substrate during a high-temperature heat treatment. This phenomenon, also termed ''film agglomeration,'' [40] has been observed for a wide range of epitaxial and polycrystalline thin films.[41–43] Film agglomeration proceeds with the nucleation and growth of holes driven by stress and capillarity effects, leading to an extremely porous, yet still contiguous film, as shown in Fig. 5(b). It has been recognized that defects play a critical role in hole formation,[40] particularly, grain-boundary grooving. Film agglomeration is also very susceptible to the film thickness in that thinner films are prone to the formation of holes.[40,43]

The observation of a microstructural instability only in the room-temperature-deposited 1273 K-annealed $AlMgB_{14}$ film suggests that this phenomenon must be associated with its two-phase microstructure. As just described, during the 1273 K-annealing process, there is a variation in tensile stress from phase to phase due to the difference in thermal expansion coefficients and elastic moduli between orthorhombic $AlMgB_{14}$ phase and tetragonal α-$FeSi_2$ phase. A grain with a lower tensile stress will lose material to grains where the tensile stress is high, giving rise to the sinking or thinning of such grains and the formation of a hole in the film. Grain sinking was shown to be the major mechanism for holes formation in thick Al film when the film was in tension.[41] Moreover, preexisting holes greater than a critical size also will initiate film agglomeration,[43] and deposition of $AlMgB_{14}$ film at room temperature inherently involves the formation of such holes due to its low density amorphous structure. Densification, as well as hole growth and coalescence, is concurrent during subsequent high-temperature annealing, resulting in the eventual development of islandlike surface morphology for the room-temperature-deposited 1273 K-annealed $AlMgB_{14}$ film.

IV. CONCLUSIONS

Al–Mg–B thin films were deposited on SiO_2/Si substrates by a nanosecond PLD technique at different substrate temperatures, the postdeposition annealing was performed at 1173 K or 1273 K for 2 h. The results of XPS, XRD, and AFM show that the as-deposited films are amorphous, and annealing at 1173 K yields either an amorphous or nanocrystalline structure. Significant formation of the orthorhombic $AlMgB_{14}$ phase with a strong (011) texture has occurred in the room-temperature and 573 K-deposited Al–Mg–B films via annealing at 1273 K, a mechanism for the (011) texture development is proposed based on minimization of interfacial free energy; however, the orthorhombic $AlMgB_{14}$ phase was not attained for the 873 K-deposited 1273 K-annealed films, which is thought to result from the high C content and nonstoichiometric composition in this film. The introduction of substantial amounts of Si into the room-temperature-deposited 1273 K-annealed $AlMgB_{14}$ film from SiO_2/Si substrate leads to the coexistence of orthorhombic $AlMgB_{14}$ phase and tetragonal α-$FeSi_2$ phase, which is thought to be responsible for the crack formation and microstructural instability observed in this film. The 573 K-deposited 1273 K-annealed $AlMgB_{14}$ film consists of single-phase orthorhombic $AlMgB_{14}$; this film is relatively smooth and free of cracks, which makes it the most suitable for mechanical and electrical characterization, such as nanoindentation, electrical conductivity measurement, etc. We plan to perform such tests in the near future on these films.

ACKNOWLEDGMENTS

This work was supported by the U.S. National Science Foundation under Grant No. DMI-0084969. The authors gratefully acknowledge the illuminating discussions with Professor Tim Sands of Purdue University. The authors also appreciate the help of N. L. Wang in XRD analysis and Dr. Bruce Cook of Ames Laboratory for providing the $AlMgB_{14}$ target material used in this study. The authors also wish to express their appreciation for the use of the characterization facilities of the Ames Laboratory. Ames Laboratory is operated by Iowa State University for the U.S. Department of Energy under Contract No. W-7405-ENG-82.

[1] S. Hwang, K. Yang, P. A. Dowben, A. A. Ahmad, N. J. Ianno, J. Z. Li, J. Y. Lin, H. X. Jiang, and D. N. Mcllroy, Appl. Phys. Lett. **70**, 1028 (1997).
[2] S. Adenwalla, P. Welsch, A. Harken, J. I. Brand, A. Sezer, and B. W. Robertson, Appl. Phys. Lett. **79**, 4357 (2001).
[3] D. Emin, Phys. Today **31**, 55 (1987).
[4] H. Werheit, Mater. Sci. Eng., B **29**, 228 (1995).
[5] C. Wood and D. Emin, Phys. Rev. B **29**, 4582 (1984).
[6] B. W. Robertson, S. Adenwalla, A. Harken, P. Welsch, J. I. Brand, P. A. Dowben, and J. P. Claassen, Appl. Phys. Lett. **80**, 3644 (2002).
[7] A. R. Badzian, Appl. Phys. Lett. **53**, 2495 (1988).
[8] B. A. Cook, J. L. Harringa, T. L. Lewis, and A. M. Russell, Scr. Mater. **42**, 597 (2000).
[9] S. M. Gorbatkin, R. L. Rhoades, T. Y. Tsui, and W. C. Oliver, Appl. Phys. Lett. **65**, 2672 (1994).
[10] S. V. Deshpande, E. Gulari, S. J. Harris, and A. M. Weiner, Appl. Phys. Lett. **65**, 1757 (1994).
[11] C. Doughty, S. M. Gorbatkin, T. Y. Tsui, G. M. Pharr, and D. L. Medlin, J. Vac. Sci. Technol. A **15**, 2623 (1997).
[12] D. Music, J. M. Schneider, V. Kugler, S. Nakao, P. Jin, M. Östblom, L. Hultman, and U. Helmersson, J. Vac. Sci. Technol. A **20**, 335 (2002).
[13] M. U. Guruz, V. P. Dravid, and Y. W. Chung, Thin Solid Films **414**, 129 (2002).
[14] K. F. Chan, C. W. Ong, C. L. Choy, and R. W. M. Kwok, J. Vac. Sci. Technol. A **17**, 2944 (1999).
[15] C. C. Klepper, R. C. Hazelton, E. J. Yadlowsky, E. P. Carlson, M. D. Keitz, J. M. Williams, R. A. Zuhr, and D. B. Poker, J. Vac. Sci. Technol. A **20**, 725 (2002).
[16] F. Kokai, M. Taniwaki, K. Takahashi, A. Goto, M. Ishihara, K. Yamamoto, and Y. Koga, Diamond Relat. Mater. **10**, 1412 (2001).
[17] A. Erdemir, G. R. Fenske, and R. A. Erck, Surf. Coat. Technol. **43/44**, 588 (1990).

[18]V. I. Matkovich and J. Economy, Acta Crystallogr., Sect. B: Struct. Crystallogr. Cryst. Chem. **26**, 616 (1970).
[19]I. Higashi and T. Ito, J. Less-Common Met. **92**, 239 (1983).
[20]R. Schmechel and H. Werheit, J. Phys.: Condens. Matter **11**, 6803 (1999).
[21]H. Werheit, U. Kuhlmann, G. Krach, I. Higashi, T. Lundström, and Y. Yu, J. Alloys Compd. **202**, 269 (1993).
[22]B. A. Cook, J. L. Harringa, T. L. Lewis, Y. B. Lee, and A. M. Russell, Adv. Mater. (Weinheim, Ger.) (to be published).
[23]Y. Lee and B. N. Harmon, J. Alloys Compd. **338**, 242 (2002).
[24]B. A. Cook, J. L. Harringa, A. M. Russell, and S. A. Batzer, Mach. Sci. Technol. **7**, 139 (2003).
[25]R. Cherukuri, M. Womack, P. Molian, A. Russell, and Y. Tian, Surf. Coat. Technol. **155**, 112 (2002).
[26]M. P. De Boer and T. M. Mayer, Mater. Res. Bull. **26**, 302 (2001).
[27]S. Veprek, J. Vac. Sci. Technol. A **17**, 2401 (1999).
[28]M. Ohring, *The Materials Science of Thin Films* (Academic, San Diego, 2002), pp. 730–732.
[29]P. R. Willmott and J. R. Huber, Rev. Mod. Phys. **72**, 315 (2000).
[30]T. L. Lewis, B. A. Cook, J. L. Harringa, and A. M. Russell, Mater. Sci. Eng. (to be published).
[31]Y. Tian, M. Womack, P. Molian, C. C. H. Lo, J. W. Anderegg, and A. M. Russell, Thin Solid Films **418**, 129 (2002).
[32]D. B. Knorr, D. P. Tracy, and K. P. Rodbell, Appl. Phys. Lett. **59**, 3241 (1991).
[33]L. Holloway, H. Laidler, N. D. Telling, and S. Z. Wu, J. Appl. Phys. **90**, 4056 (2001).
[34]A. R. Phani, J. E. Krzanowski, and J. J. Nainaparampil, J. Mater. Res. **17**, 1390 (2002).
[35]I. Higashi, M. Kobayashi, S. Okada, K. Hamano, and T. Lundström, J. Cryst. Growth **128**, 1113 (1993).
[36]Y. C. Feng, D. E. Laughlin, and D. N. Lambeth, J. Appl. Phys. **76**, 7311 (1994).
[37]Q. Wei, J. Sankar, A. K. Sharma, Y. Yamagata, and J. Narayan, J. Vac. Sci. Technol. A **19**, 311 (2001).
[38]A. M. Russell, B. A. Cook, J. L. Harringa, and T. L. Lewis, Scr. Mater. **46**, 629 (2002).
[39]A. H. Reader, A. H. van Ommen, P. J. W. Weijs, R. A. M. Wolters, and D. J. Oostra, Rep. Prog. Phys. **56**, 1397 (1993).
[40]D. J. Srolovitz and M. G. Goldiner, J. Met. 31 (1995).
[41]N. Kristensen, F. Ericson, J. Schweitz, and U. Smith, J. Appl. Phys. **69**, 2097 (1991).
[42]E. Jiran and C. V. Thompson, Thin Solid Films **208**, 23 (1992).
[43]A. Seifert, A. Vojta, J. S. Speck, and F. F. Lange, J. Mater. Res. **11**, 1470 (1996).